Title
Ab initio calculation of molecular aggregation effects: a Coumarin-343 case study.

Journal
The journal of physical chemistry. A, 117(43)

ISSN
1089-5639

Authors
Lee, Donghyun
Greenman, Loren
Sarovar, Mohan
et al.

Publication Date
2013-10-01

DOI
10.1021/jp405152h

Peer reviewed

Ab-Initio Calculation of Molecular Aggregation Effects: a Coumarin-343 Case Study

Donghyun Lee,[1] Loren Greenman,[1] Mohan Sarovar,[2] and K. Birgitta Whaley[1,*]

[1]*Department of Chemistry, University of California, Berkeley, California, USA*
[2]*Scalable and Secure Systems Research, Sandia National Laboratories, MS 9158, 7011 East Avenue, Livermore, California 94550 USA*

(Dated: August 26, 2019)

ABSTRACT: We present time-dependent density functional theory (TDDFT) calculations for single and dimerized Coumarin-343 molecules in order to investigate the quantum mechanical effects of chromophore aggregation in extended systems designed to function as a new generation of sensors and light-harvesting devices. Using the single-chromophore results, we describe the construction of effective Hamiltonians to predict the excitonic properties of aggregate systems. We compare the electronic coupling properties predicted by such effective Hamiltonians to those obtained from TDDFT calculations of dimers, and to the coupling predicted by the transition density cube (TDC) method. We determine the accuracy of the dipole-dipole approximation and TDC with respect to the separation distance and orientation of the dimers. In particular, we investigate the effects of including Coulomb coupling terms ignored in the typical tight-binding effective Hamiltonian. We also examine effects of orbital relaxation which cannot be captured by either of these models.

Keywords: light harvesting, Frenkel Excitons, electronic coupling, ideal dipole approximation, TDDFT

I. INTRODUCTION

The geometry of chromophore aggregates influences how they couple to one another, which in turn determines the electronic properties of the extended system. Deliberate control over the positions and orientations of chromophores can thereby be used to achieve specific properties such as efficient energy transfer[1]. Light harvesting in photosynthesis is an example from nature of how chromophores embedded in proteins have been optimized by evolution to capture light over a specific spectrum and to efficiently transfer the excitation energy to the photosynthetic reaction center[2–5]. In designing synthetic light harvesting antennae for organic sensors or photovoltaics, it is critical to understand how the structural and orientational properties of the chromophore arrays affects their coupling, and hence their excitonic and optical properties[6–11]. Importantly, recent work has suggested that quantum mechanical effects play a key role in the high efficiency of biological excitation energy transfer (EET)[12–15]. Understanding the details of the quantum mechanical coupling between chromophores is an important step towards probing and exploiting any beneficial effects of quantum mechanical coherence in energy transfer.

Due to its spectroscopic attributes and small size, coumarin-343 (see Fig. 1) is a molecule of particular interest for use in virus-templated synthetic light harvesting complexes, using *e.g.* the tobacco mosaic virus (TMV) protein scaffold[16]. The TMV protein monomers undergo self-assembly to form complex structures such as helices and stacked disks[17]. The assembled TMV can be made into a light harvesting array by covalently attaching chromophores such as coumarin-343 onto the protein[16,18–20]. The stacked disks and helical arrays of chromophores act as aggregate systems with optical properties (spectral width, peak absorption frequency) that differ from those of the free chromophore. It is possible to exercise a fine degree of control over these optical properties by changing the concentration of chromophores and the positions at which they are attached[21].

Conventionally the interaction between excited states of nearby chromophores is modeled using a tight-binding Hamiltonian of the form[5,22],

$$H = \sum_{i=1}^{N} \epsilon_i \sigma_i^\dagger \sigma_i + \sum_{i \neq j}^{N} J_{i,j} \sigma_i^\dagger \sigma_j, \tag{1}$$

where ϵ_i is the transition energy of chromophore i, $J_{i,j}$ is the coupling between chromophores i and j, $\sigma_i^\dagger \equiv \left|\psi_1^i\right\rangle \left\langle\psi_0^i\right|$ is a Pauli creation operator for an excitation on chromophore i, and $\sigma_i \equiv \left|\psi_0^i\right\rangle \left\langle\psi_1^i\right|$ is a Pauli annihilation operator for an excitation on chromophore i. In this approach each molecule is treated as a two-level system and the number of excitations is conserved. This truncated description of the intermolecular Hamiltonian is often referred to as the Frenkel Hamiltonian (or Frenkel exciton model) in the Heitler-London approximation[23]. Such effective Hamiltonian descriptions constitute the only feasible approach to study large molecular aggregates, since *ab-initio* methods cannot be scaled to such large systems. However, some of the parameters entering the effective Hamiltonian descriptions can be calculated using *ab-initio* methods. For instance, the coupling between chromophores ($J_{i,j}$), which is well-approximated by a Coulombic interaction between the transition densities of chromophores i and j, can be calculated

exactly using the transition density cube (TDC) method[24]. The most common way to approximate this coupling is by the ideal dipole approximation (IDA)[25] which treats the $1/r$ interaction between the two densities as an interaction between the dipole moments of the transition densities; several papers have compared the accuracy of the IDA to the more complete TDC description in various molecules [26–28]. The effective Hamiltonian in Eq. (1) relies on the approximation that the aggregate wavefunction can be reasonably constructed from the product of monomer wavefunctions (a Heitler-London-type picture). However such effective Hamiltonian descriptions may also neglect other potentially important aspects of the intermolecular interactions. In particular, Eq. (1) does not include electron exchange between the chromophores, nor does it allow for relaxation of the monomer wavefunctions. To go beyond this approximate description requires making detailed electronic structure calculations on the aggregate, and this is what we undertake in this study.

In the following sections we present time-dependent density functional theory (TDDFT) results for coumarin-343 and compare them to results from the IDA and TDC. We also compare to an effective Hamiltonian that we obtain from expressing the molecular Hamiltonian in a basis constructed from products of monomer wavefunctions. TDDFT provides a middle ground between accuracy and computational expense, and we have performed some benchmarking calculations to determine the quality of TDDFT for coumarin.

The results presented here are similar in spirit to a number of recent *ab-initio* studies of excited states of molecular aggregates, and we briefly review some of these studies here. Firstly, Ref.[29], which perhaps has the most overlap with the results in this work, develops a method referred to as TrEsp for using *ab-initio* calculations of charge and transition densities for monomers to determine energies of excited states of coupled chromophores. Next, some recent papers, *e.g.*,[30,31], have examined the various components of electronic coupling in condensed media using *ab-initio* methods, separately characterized through-bond and through-space contributions, and analyzed the effects of solvent properties on these. Finally, several works have examined the aggregation mechanisms and subsequent excited states of molecular aggregates of dimers and extended systems using *ab-initio* methods[32–36]. These studies concentrate on aggregates common in molecular crystals (*e.g.*, perylene bisimide (PBI) aggregates) and as a result focus on very densely packed systems; typical inter-molecular separation distances studied in these works are in the range 2-8Å. In such self-assembling aggregates the mechanisms that dictate aggregation geometries and intermolecular potentials – *e.g.*, dispersion forces – are critical to understanding excited state energies. In contrast, in the papers cited above and in this work the focus is on molecular aggregates found in biomimetic or biological systems. In such systems the inter-molecular separation is typically larger, and critically, the forces that dictate aggregation are mostly due to external influences such as protein scaffolds. Therefore in such systems the intermolecular potentials play a smaller role although as we show below they cannot be ignored completely.

An outline of the remainder of the paper follows. In section III A, we present these benchmarking calculations and give the TDDFT transition energies and transition dipoles for a single coumarin-343 chromophore. These are the simplest parameters which can be used in Eq. (1). Then, in section III B, we explore using TDDFT the energetics resulting from coupling between two dyes at a number of separation distances and orientations. We compare the TDDFT exciton splitting energies to splittings calculated by approximate methods, and also examine the effects of aggregation on exciton energies and wave functions, in particular, the role of orbital relaxation and deviations from the solutions to the Heitler-London description of monomer coupling.

II. METHODS

The geometries of all the monomers considered in this report have been minimized using the B3LYP/6-31G* level of theory[37–40]. Single-point ground and excited-state energy calculations were then performed using TDDFT[41,42] with the M06-HF[43], M11[44], M11-L[45], and PBE[46,47] functionals and the 6-31G*[38–40], 6-31+G*[38–40,48], and 6-311G**[49,50] basis sets. EOM-CCSD[51–53] calculations were performed to benchmark the density functionals, and multi-configurational self-consistent-field (MCSCF)[54] calculations were used to examine the presence of multireference character. The polarized continuum model (PCM)[55] was used to model the effects of water solvation. Range-corrected TDDFT[56] was also used to determine the energetic order of the charge-transfer states, which TDDFT predicts to be too low in energy. All calculations were performed using the GAMESS electronic structure package[57,58], except for the transition density cube files (the one particle transition density projected onto a 3 dimensional cartesian grid) which were obtained from Q-Chem[59].

The calculations in this paper use a modified coumarin-343 molecule which has an amide group that is necessary for attaching the dye on to the TMV substrate. For simplicity, in this work we shall refer to this modified molecule as coumarin-343-MA (coumarin-343-methylamide).

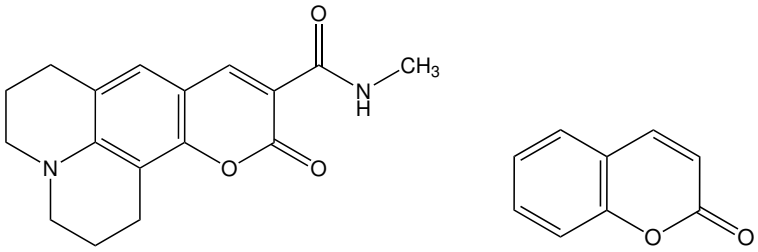

(a) Coumarin-343-MA (b) Coumarin

FIG. 1: (a) Structure of coumarin-343-MA, modified for attachment to TMV substrate. (b) The smaller coumarin molecule, on which we performed larger and more accurate calculations to benchmark the density functionals we used.

III. RESULTS AND DISCUSSION

A. Single-chromophore benchmarking studies and parameter determintation

In order to choose an appropriate density functional and basis set for coumarin-343-MA, we first ran benchmarking calculations on coumarin (see Fig. 1). We use the transition energy and the transition dipole moment to gauge accuracy, since these are the key quantities relevant in many effective Hamiltonian approaches. Four TDDFT functionals were compared with the more accurate EOM-CCSD method, and the results are summarized in Table I.

TABLE I: Density functional benchmarking for coumarin in the gas phase. The TDDFT excitation energies and oscillator strengths (f) for five functionals and three basis sets were compared with the EOM-CCSD results. The B3LYP functional matched both the excitation energy and the oscillator strength of EOM-CCSD within our tolerance. The results show only a very weak dependency to the choice of basis set.

			1^{st} Excited State		2^{nd} Excited State	
Basis Set	Functional	Ground State Energy [Ha]	Exc. Energy [eV]	f	Exc. Energy [eV]	f
6-31G*	M06-HF	−496.8747	4.415	0.000	4.780	0.215
	M11	−496.7467	4.606	0.180	4.809	0.000
	M11-L	−496.8800	4.152	0.052	4.407	0.000
	PBE	−496.4380	3.625	0.000	3.822	0.060
	B3LYP	−496.7418	4.182	0.111	4.396	0.000
	EOM-CCSD	−495.5607	4.563	0.089	5.126	0.000
6-31+G*	M06-HF	−496.8921	4.457	0.000	4.699	0.241
	M11	−496.7619	4.548	0.197	4.848	0.000
	M11-L	−496.8908	4.078	0.055	4.414	0.000
	PBE	−496.4571	3.705	0.000	3.782	0.062
	B3LYP	−496.7612	4.129	0.119	4.453	0.000
	EOM-CCSD	−495.5870	4.497	0.098	5.121	0.000
6-311G**	M06-HF	−497.0182	4.481	0.000	4.707	0.239
	M11	−496.8850	4.552	0.181	4.775	0.000
	M11-L	−497.0357	4.090	0.054	4.320	0.000
	PBE	−496.5658	3.618	0.000	3.781	0.060
	B3LYP	−496.8725	4.132	0.111	4.383	0.000
	EOM-CCSD	−495.7996	4.502	0.095	5.068	0.000

For each basis set, the EOM-CCSD method predicts a first excitation energy of 4.5-4.6 eV and an oscillator strength of 0.09-0.10. The M11 functional is able to reproduce the excitation energy well, but it significantly overestimates the oscillator strength and transition dipoles. Since the accuracy of the transition dipole directly affects the accuracy of the chromophore couplings, the B3LYP functional offered a better combination of accuracy in the energetics and the transition dipoles. There is not a large basis set effect for the basis sets considered, and so we performed further calculations at the B3LYP/6-31G* level of theory.

We also check for multireference character, which occurs when multiple Slater determinants are needed to accurately express the zeroth-order wavefunction. This is common for large or conjugated molecules. MCSCF calculations were run on coumarin-343-MA using an active space of 7 electrons in 7 π-orbitals. The natural orbital occupation numbers, which are the eigenvalues of the one-electron reduced density operator[60],

$$\gamma(r_1, r_1') = N \int \dots \int \psi^*(r_1, r_2 \dots r_N)\psi(r_1', r_2 \dots r_N)\mathrm{d}r_2 \dots \mathrm{d}r_N, \tag{2}$$

are useful for determining multireference character; occupation numbers that deviate significantly from 0.0 or 2.0 indicate that a multireference wavefunction is needed. We find that the occupation numbers of the occupied and unoccupied orbitals were all greater than 1.9 or less than 0.12. This indicates that there is little multireference character for this dye and so the benchmark calculations and TDDFT calculations are both adequate.

TABLE II: TDDFT results for Coumarin-343. The ground-state and excitation energies, transition dipoles, and oscillator strengths are given for each functional using the 6-31G* basis set. The PBE functional is not included as it performed poorly in the benchmark calculations on the coumarin molecule. The final column gives the B3LYP result using a continuum model to describe solvation in water.

		M06-HF	M11	M11-L	B3LYP	B3LYP (Water)
Ground State Energy [Ha]		−993.5938	−993.3408	−993.5986	−993.2967	−993.3128
1^{st} Excitation Energy [eV]		3.927	3.839	3.445	3.465	3.199
Transition Dipole [Debye]	x	0.062	0.070	−0.014	0.000	−0.076
	y	−0.022	0.114	−0.018	0.000	0.034
	z	7.228	7.029	6.101	6.706	7.611
Oscillator Strength		0.778	0.729	0.486	0.591	0.703

The B3LYP/6-31G* excitation energies and transition dipoles for coumarin-343-MA are given in Table II, together with results for the other functionals. At this level of theory, the first excitation energy is 3.465 eV and the oscillator strength is 0.591. The transition dipole between the ground and first excited states of coumarin-343-MA is pictured in Fig. 2(a). We see that the transition dipole lies flat along the plane of the molecule, on the axis formed between the center of the molecule and the nitrogen atom of the amide group.

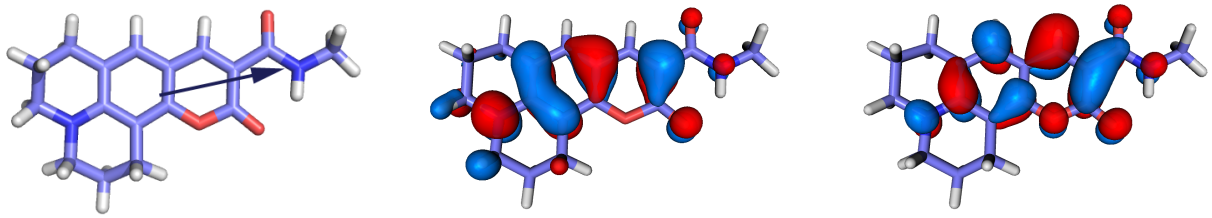

(a) transition dipole moment (b) HOMO (c) LUMO

FIG. 2: (a) The transition dipole of coumarin-343-MA calculated at the TD-B3LYP/6-31G* level of theory. (b) The highest occupied molecular orbital (HOMO) of coumarin-343-MA. (c) The lowest unoccupied molecular orbital (LUMO) of coumarin-343-MA.

B. Two-dye coupling calculations

Now we turn to assessing the magnitude of the coupling between excited states of pairs of molecules, where these are denoted as A and B. Using the benchmarking studies described in the previous subsection, we calculated the energetics of two coumarin-343-MA molecules at various separation distances and different relative orientations, using the B3LYP/6-31G* functional and basis set. With one molecule aligned with its molecular axis along the $\phi_A = 0$ azimuth in the xy-plane, the relative orientations are defined by the two polar angles θ_A, θ_B and the second azimuthal angle ϕ_B, where the polar angle is the angle between the long axis of the molecule and a laboratory fixed z-axis (see Appendix A).

In the following we will use E_i ($\tilde{E}_i$) to denote the monomer (dimer) energies calculated using TDDFT.

For a homo-dimer, the tight-binding effective Hamiltonian of Eq. (1) reduces to

$$\hat{H} = \begin{array}{c} \\ \langle 10| \\ \langle 01| \end{array} \begin{array}{c} \begin{array}{cc} |10\rangle & |01\rangle \end{array} \\ \begin{pmatrix} \epsilon_0 & J \\ J & \epsilon_0 \end{pmatrix} \end{array} \tag{3}$$

in a basis of excitations on the left ($|10\rangle$) and right ($|01\rangle$) chromophores, where $\epsilon_0 = E_1 - E_0$ is the first excitation energy of the monomer and J is the coulombic coupling between monomers. As mentioned in the Introduction, in the

absence of exchange this coupling can be captured as the Coulomb interaction between transition densities (e.g. in the TDC method), and this can be further approximated as a dipole-dipole interaction (as in the IDA). Diagonalizing the matrix in Eq. (3) results in delocalized exciton states with symmetrically split energies, also known as Davydov splitting[61],

$$|\psi_{\pm}\rangle = \frac{|10\rangle \pm |01\rangle}{\sqrt{2}} \qquad\qquad \epsilon_{\pm} = \epsilon_0 \pm J. \tag{4}$$

W emphasize that this theory predicts a symmetric splitting of the exciton energies according to Eq. (4). In this section we will assess the degree to which TDDFT calculations agree with the tight-binding effective Hamiltonian description of the excited states of the coumarin-343-MA homo-dimer. In particular, we will examine three specific aspects, for various chromophore separation distances and chromophore orientations: (i) we will compare the TDDFT description of the Coulombic coupling magnitude J to the magnitudes provided by IDA and TDC, (ii) we will assess the validity of the form of the symmetric eigenstates given in Eq. (4), and (iii) we will assess the validity of the symmetric splitting of eigenenergies given in Eq. (4).

1. Coulomb coupling energy

Fig. 3 shows the splitting of the excited state energies ($\frac{\tilde{E}_2 - \tilde{E}_1}{2}$) for TDDFT as a function of the inter-chromophore separation distance for three different relative orientations. For comparison, we have also plotted the energetic splitting predicted by Eq. (4) when the Coulomb coupling J is calculated using the IDA and TDC methods. Comparison of this predicted energetic splitting is the most consistent methods for comparing the three methods.

From Fig. 3 we see that the numerically integrated TDC method agrees very well with the TDDFT calculations, while the IDA over-predicts for the 0° relative orientation (parallel and anti-parallel) and under-predicts for the 30° relative orientation. As the intermolecular separation increases, the IDA values begin to qualitatively match the TDDFT/TDC values after 12Å separation, however the convergence of the percent error is still quite slow. The percent error of the IDA splitting decreases to 10% only after 30Å separation (averaged over the three orientations). This shows that the IDA can be a poor description of Coulombic coupling for inter-chromophoric distances that are less than 30Å. More sophisticated methods such as TDC should be used in such cases. This conclusion is in agreement with Refs. [26–28].

Calculations where the relative orientation between dimers is explored while keeping the distance separation fixed were also done. The results confirm that the TDC can reliably predict the energetic splittings. TDC systematically outperforms IDA, and is also able to predict the correct splitting in geometries where the molecules are nearly in contact with one another. Details of this analysis may be found in the appendix.

2. Exciton energies and site-energy shifts

Fig. 4 shows TDDFT excitation energies as a function of inter-chromophore distance at three different orientations. The most striking feature of these plots is that the excitation energies split asymmetrically from the energy of the monomer excited state (indicated by the dashed line). This is in disagreement with the tight-binding effective Hamiltonian which predicts a symmetric splitting of the energies around the monomer energy (see Eq. (4)).

To explain this discrepancy we must re-examine the full molecular Hamiltonian of the coupled chromophore system. In a basis of single-chromphore ground states and single excitations,

$$|00\rangle = \left|\psi_0^A\right\rangle \otimes \left|\psi_0^B\right\rangle \qquad |10\rangle = \left|\psi_1^A\right\rangle \otimes \left|\psi_0^B\right\rangle$$
$$|11\rangle = \left|\psi_1^A\right\rangle \otimes \left|\psi_1^B\right\rangle \qquad |01\rangle = \left|\psi_0^A\right\rangle \otimes \left|\psi_1^B\right\rangle$$

where $\left|\psi_i^A\right\rangle \otimes \left|\psi_j^B\right\rangle$ indicates a direct product wavefunction between molecule A in state i and molecule B in state j, the Born-Oppenheimer molecular Hamiltonian is written as[62]

$$\hat{H} = \begin{array}{c} \\ \langle 00| \\ \langle 10| \\ \langle 01| \\ \langle 11| \end{array} \begin{array}{c} \begin{array}{cccc} |00\rangle & |10\rangle & |01\rangle & |11\rangle \end{array} \\ \begin{pmatrix} 2E_0 + J_{\text{gs}}^{\text{gs}} & J_{\text{trans}}^{\text{gs}} & J_{\text{gs}}^{\text{trans}} & J_{\text{trans}}^{\text{trans}} \\ J_{\text{trans}}^{\text{gs}} & E_0 + E_1 + cJ_{\text{es}}^{\text{gs}} & J_{\text{trans}}^{\text{trans}} & J_{\text{es}}^{\text{trans}} \\ J_{\text{gs}}^{\text{trans}} & J_{\text{trans}}^{\text{trans}} & E_0 + E_1 + cJ_{\text{gs}}^{\text{es}} & J_{\text{trans}}^{\text{es}} \\ J_{\text{trans}}^{\text{trans}} & J_{\text{es}}^{\text{trans}} & J_{\text{trans}}^{\text{es}} & 2E_1 + J_{\text{es}}^{\text{es}} \end{pmatrix} \end{array} \tag{5}$$

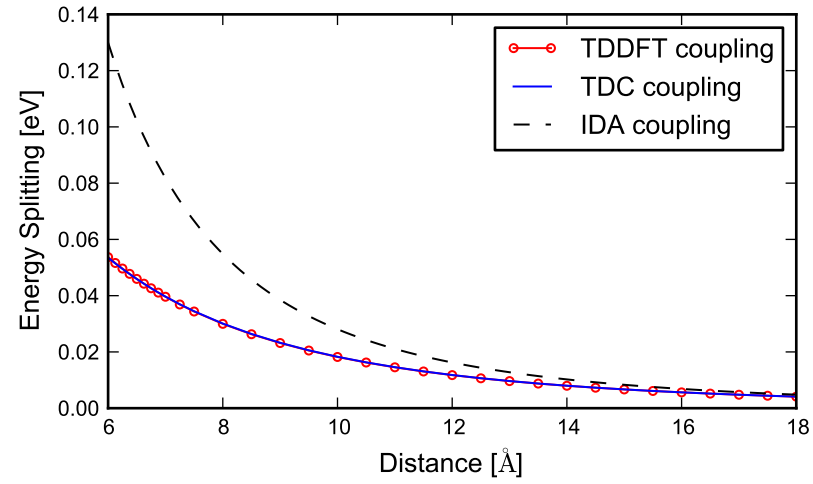

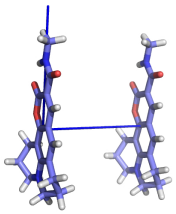

Parallel-0°

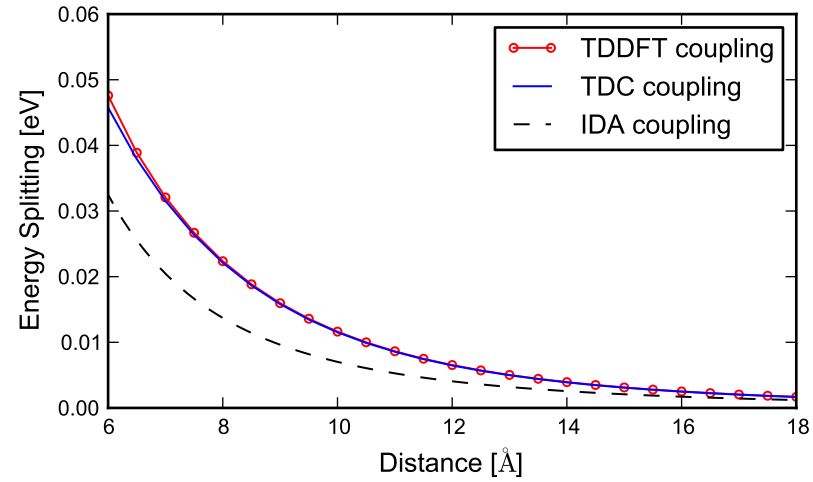

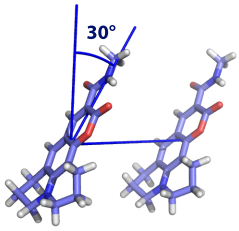

Parallel-30°

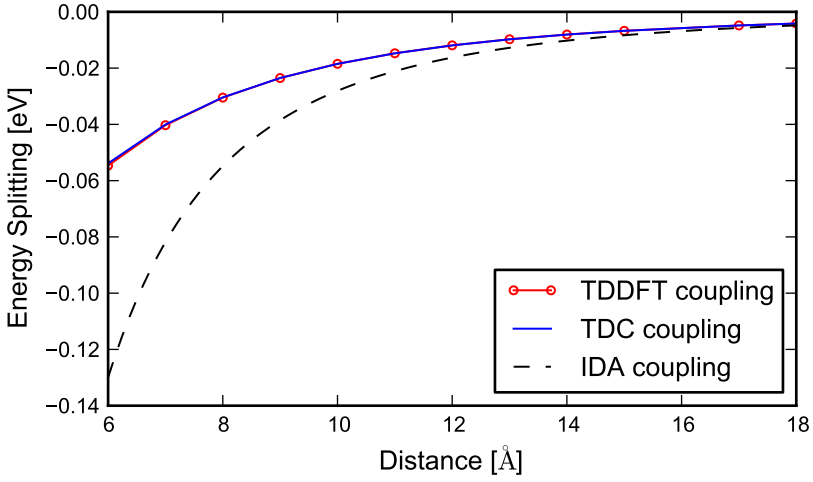

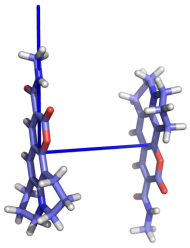

Anti-Parallel-0°

FIG. 3: The energy splittings between the dimer excited states are shown for TDDFT, TDC and IDA calculations. The TDDFT points show $\frac{\tilde{E}_2-\tilde{E}_1}{2}$, while the TDC and IDA lines show $\frac{\epsilon_+-\epsilon_-}{2}$ with the J coupling calculated using the respective approximation. The TDC and TDDFT predictions mostly overlap.

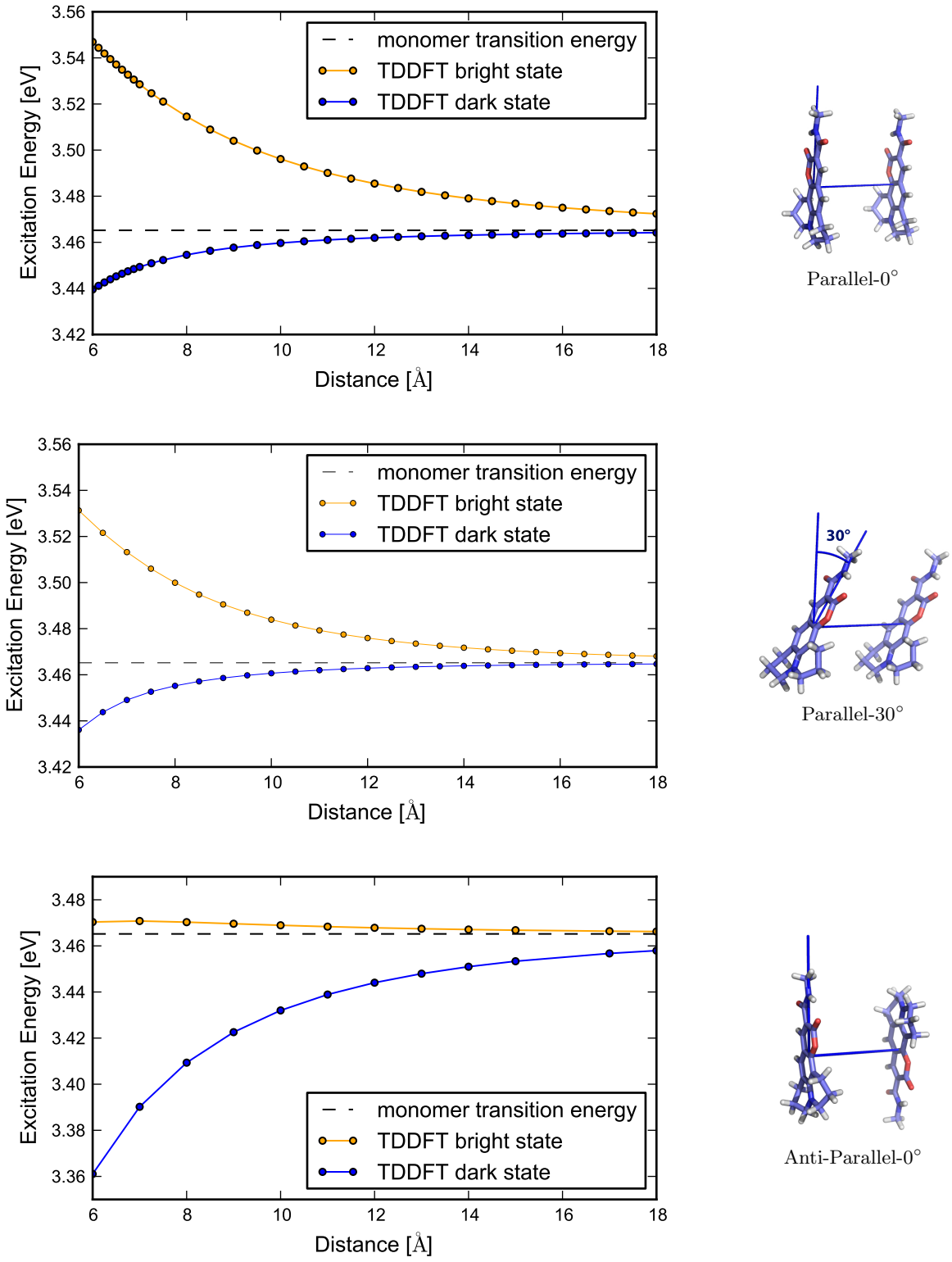

FIG. 4: TDDFT excitation energies ($\tilde{E}_1 - \tilde{E}_0$ and $\tilde{E}_2 - \tilde{E}_0$) for the coupled excited states of the coumarin-343-MA dimer. Orientation of the dimer is shown to the right. Erroneous charge transfer states are not shown, since they do not mix into the optical states (see appendix for details).

where E_i are the relevant monomer energies. Ignoring the effects of quantum mechanical exchange, which we have determined from the TDDFT calculations to be small at these distances, the coupling terms J_i^j indicate coulomb integrals between either a charge or transition density on molecule A and either a charge or transition density on molecule B, i.e.

$$J_{\mathrm{i}}^{\mathrm{j}} = \int \rho_i^A(r_1) \frac{1}{|r_1 - r_2|} \rho_j^B(r_2) \mathrm{d}r_1 \mathrm{d}r_2. \tag{6}$$

with i, j equal to either *gs* (ground state charge density), *es* (excited state charge density), or *trans* (transition density). The charge densities and transition densities are defined for molecule A as

$$\rho_{\mathrm{gs}}^A(r_1) = N \int \ldots \int \psi_0^{A*}(r_1, r_2 \ldots r_N) \psi_0^A(r_1, r_2 \ldots r_N) \mathrm{d}r_2 \ldots \mathrm{d}r_N \times \sum_{n \in A} Z_n \delta(R_n - r_1) \tag{7}$$

$$\rho_{\mathrm{es}}^A(r_1) = N \int \ldots \int \psi_1^{B*}(r_1, r_2 \ldots r_N) \psi_1^B(r_1, r_2 \ldots r_N) \mathrm{d}r_2 \ldots \mathrm{d}r_N \times \sum_{n \in B} Z_n \delta(R_n - r_1) \tag{8}$$

$$\rho_{\mathrm{trans}}^A(r_1) = \int \ldots \int \psi_0^{A*}(r_1, r_2 \ldots r_N) \psi_1^A(r_1, r_2 \ldots r_N) \mathrm{d}r_2 \ldots \mathrm{d}r_N, \tag{9}$$

and similarly for molecule B, where Z_n and R_n correspond to the charge and positions of the nuclei in their respective molecules, and N is the total number of electrons in a molecule. The coefficient c is a parameter used to scale the magnitude of the ground-state/excited-state Coulomb integral (see discussion below).

In order to reduce this Hamiltonian into the tight-binding effective Hamiltonian in Eq. (3) a number of approximations must be made. Firstly, the Coulomb integrals are assumed to be much smaller than the energetic differences and therefore the matrix in Eq. (5) is approximated as block diagonal, with each block labeled by the number of excited states. Explicitly, $J_i^j \ll E_1 - E_0$ but $J_{\mathrm{es}}^{\mathrm{gs}} \approx J_{\mathrm{gs}}^{\mathrm{es}}$, and therefore we can ignore all off-diagonal terms except for those coupling $|10\rangle$ and $|01\rangle$. This approximation is sometimes referred to as the Heitler-London approximation in the literature [63]. Typically, the intermolecular Coulomb interaction terms are ignored i.e., one assumes that $J_{\mathrm{gs}}^{\mathrm{gs}} \approx J_{\mathrm{es}}^{\mathrm{gs}} \approx J_{\mathrm{gs}}^{\mathrm{es}} \approx 0$, and then the only Coulomb interaction terms that remain are the $J_{\mathrm{trans}}^{\mathrm{trans}}$ terms. Under this approximation the Hamiltonian in the single excitation subspace (after a shift of the diagonal energies by $2E_0$) is the one given in Eq. (3),

$$\hat{H} - 2E_0 = \begin{array}{c} \\ \langle 10| \\ \langle 01| \end{array} \begin{array}{c} \begin{array}{cc} |10\rangle & |01\rangle \end{array} \\ \begin{pmatrix} \epsilon_0 & J_{\mathrm{trans}}^{\mathrm{trans}} \\ J_{\mathrm{trans}}^{\mathrm{trans}} & \epsilon_0 \end{pmatrix} \end{array} \tag{10}$$

with $\epsilon_0 = E_1 - E_0$.

We assess the validity of these approximations by evaluating the expanded 4×4 effective Hamiltonian Eq. (5). In order to calculate the matrix elements of this larger Hamiltonian we use Mulliken partial atomic charges[64] for the ground state and excited state densities instead of density cubes. This is because density cube calculations are not constrained to reproduce the correct multipole expansion of the electron densities. These errors can be corrected for the transition density, as shown by Kreuger et al.[24], however the errors are more pronounced in the ground state and excited state densities, making them sensitive to the choice of grid resolution. In Fig. 5, we show the results of using this expanded effective Hamiltonian. It is evident from Fig. 5 that we are able to reproduce the asymmetric shifts in excitonic energies using Eq. (5).

The primary effects that invalidate the approximations leading to Eq. (10) are electrostatic in nature. The neglect of the $J_{\mathrm{trans}}^{\mathrm{es}}, J_{\mathrm{trans}}^{\mathrm{gs}}, J_{\mathrm{es}}^{\mathrm{trans}}, J_{\mathrm{es}}^{\mathrm{trans}}$ and the $J_{\mathrm{trans}}^{\mathrm{trans}}$ terms coupling the ground state $|00\rangle$ to the two-exciton state $|11\rangle$ (Heitler-London approximation) is valid since these are much less than $E_1 - E_0$ at all the inter-chromophore distance scales we examined. However, the electrostatic corrections to the diagonal elements of Eq. (5), $J_{\mathrm{gs}}^{\mathrm{gs}}, J_{\mathrm{es}}^{\mathrm{gs}}, J_{\mathrm{gs}}^{\mathrm{es}}, J_{\mathrm{es}}^{\mathrm{es}}$, are significant and cannot be neglected. These are shifts to monomer energies due to the presence of the charges on the other chromophore. These electrostatic shifts are dependent on the inter-chromophoric distance and the exact orientation of the chromophores. Using the Mulliken partial atomic charge approach we are able to capture these electrostatic shifts and thereby get very good agreement with the TDDFT energies. The static dipole for the ground state and excited state both lie nearly parallel to the transition dipole moment. Consequently, the direction of the shifts is consistent with what is expected from the interaction of two electronic dipoles - the parallel dimers have a repulsive electrostatic effect while the anti-parallel dimers have an attractive effect.

While the asymmetric splitting is immediately captured by including these electrostatic distance-dependent shifts, scaling the ground-state/excited-state coulomb integrals by $c = 0.66$ is necessary in order to achieve quantitative agreement with the TDDFT energies. The value of this scaling factor is specific to a chromophore pair, but once

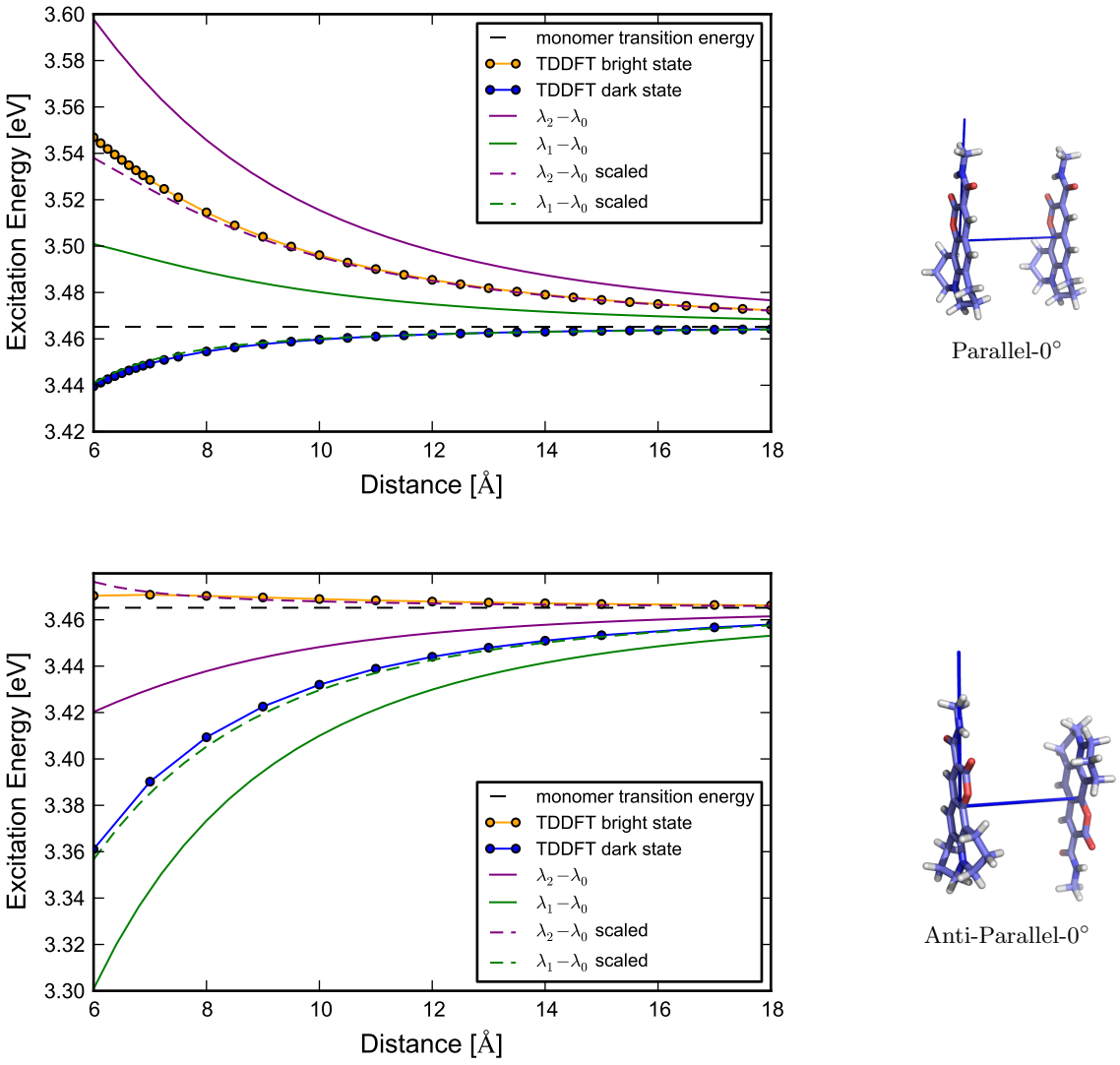

FIG. 5: The energy levels calculated using TDDFT are together with the excited states of the 4x4 Hamiltonian in Eq. (5). For the latter, the excited states are plotted as $\lambda_1 - \lambda_0$ and $\lambda_2 - \lambda_0$ where λ_i is the i^{th} eigenvalue.

determined for a particular orientation and distance separation, it holds for nearly all inter-chromophore separations and orientations. We have confirmed this by explicit calculation of energies at additional orientations and distances not presented in Fig. 5. We interpret this parameter as the screening of the Coulomb integral by the other electrons in the molecular dimer.

We remark here that similar electrostatic shifts of proximal chromophores were identified in Ref.[65]. Such electrostatic shifts to monomer energies can be a significant source of disorder in multi-chromophoric assemblies. It is widely accepted that protein residues cause energetic shifts that are important for providing a favorable energetic landscape for energy transfer[66]. Our results indicate that in addition to the effect of the proteins, the electrostatic environment provided by neighboring chromophores should also be taken into account when calculating energetic shifts and disorder in multi-chromophoric arrays. From a design perspective, this implies that the exact orientation and placement of chromophores are important not only for the precise engineering of the excitonic coupling between chromophores but also for engineering the energetic landscape.

We note that the electrostatic shifts identified here can be strongly affected by the polarity of the solvent[30]. In particular, charge screening by a polar solvent can reduce the value of electrostatic integrals such as $J_{\text{gs}}^{\text{es}}$. These integrals are likely to be more suppressed than the transition density integrals, e.g. $J_{\text{trans}}^{\text{trans}}$, and therefore the energy shifts can be suppressed even though the excitonic coupling (which is largely determined by $J_{\text{trans}}^{\text{trans}}$) may be only marginally

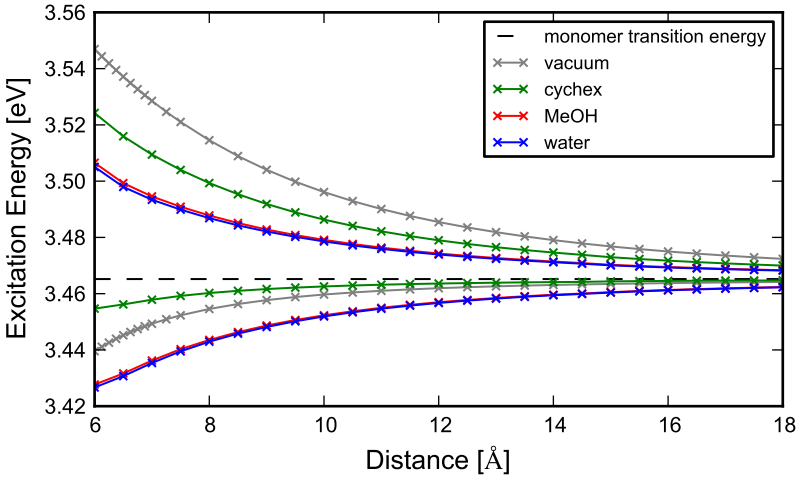

FIG. 6: TDDFT excitation energies ($\tilde{E}_1 - \tilde{E}_0$ and $\tilde{E}_2 - \tilde{E}_0$) for the coupled excited states of the coumarin-343-MA dimer in various solvent environments (modeled using PCM). Only results for the parallel oriented dimer are shown.

effected by solvent screening[31]. To demonstrate this we calculated the excitations energies of the coumarin-343-MA homo-dimer in various solvent environments modeled using a polarizable continuum model (PCM). The results are shown in Fig. 6 for the parallel oriented dimer. Clearly, as the polarity of the solvent increases the asymmetry of the excitation energy splitting around the monomer energy decreases. This demonstrates that it is important to integrate information about the solvent environment when modeling excitonic properties of molecular aggregates; solvent polarity will dictate the amount of influence electrostatic effects have on excitonic energies.

3. Exciton wave functions

We now investigate the character of the TDDFT excited states to examine whether they are well described by products of monomer wavefunctions, as predicted by Eq. (4). The tight-binding effective Hamiltonian description of the excited states can break down if either the dimer orbitals change with respect to the monomer orbitals, or the nature of the excited state changes significantly as a function of distance. The TDDFT excited states are written as linear combinations of basis functions which represent single-particle excitations from the DFT ground state. If the coefficients of this linear expansion are distance-dependent, the predictions of the effective Hamiltonian in Eq. (3) are invalid. This is because the exciton wave functions in Eq. (4) are constructed from symmetric and anti-symmetric combinations of the monomer states (i.e. Eq. (4)), and are therefore independent of the magnitude of the coupling energy J and hence of the inter-chromophoric separation. Fig. 7 shows these coefficients for the bright state of the parallel orientation of the monomers as a function of distance. We see from this figure that the nature of the TDDFT excited state is relatively constant as a function of distance, until we get to small separation distances (below 8 Å). In particular, the dominant single-particle excitation, that from the highest occupied molecular orbital (HOMO) to the lowest unoccupied molecular orbital (LUMO) on each monomer, begins to change at intermolecular distances less than 8 Å. However, some of the other minor excitations which contribute to the TDDFT excited state begin to change gradually as a function of distance already at 12 Å. Some of the single-particle excitations which contribute below 7 Å represent charge-transfer excitations from molecule A to molecule B. The existence of charge transfer, especially between 6 and 7 Å, is a feature present also for range-corrected TDDFT functionals (see Appendix). However, it should be noted that TDDFT is known to be inaccurate in describing charge transfer, so we do not regard its quantitative predictions for charge transfer at these distance scales to be reliable.

In Fig. 8, we show the overlap integral of the monomer molecular orbitals and the corresponding dimer orbitals,

$$\int \phi_n^{\text{dimer}}(r)\phi_n^{\text{monomer}}(r)\mathrm{d}r. \tag{11}$$

In the limit of infinite separation between the two dyes, each dimer molecular orbital is doubly degenerate, possessing unit overlap with a corresponding monomer molecular orbital. For the HOMO and LUMO, which are the most important orbitals in the bright state (Fig. 7), the correspondence between monomer and dimer MOs is almost

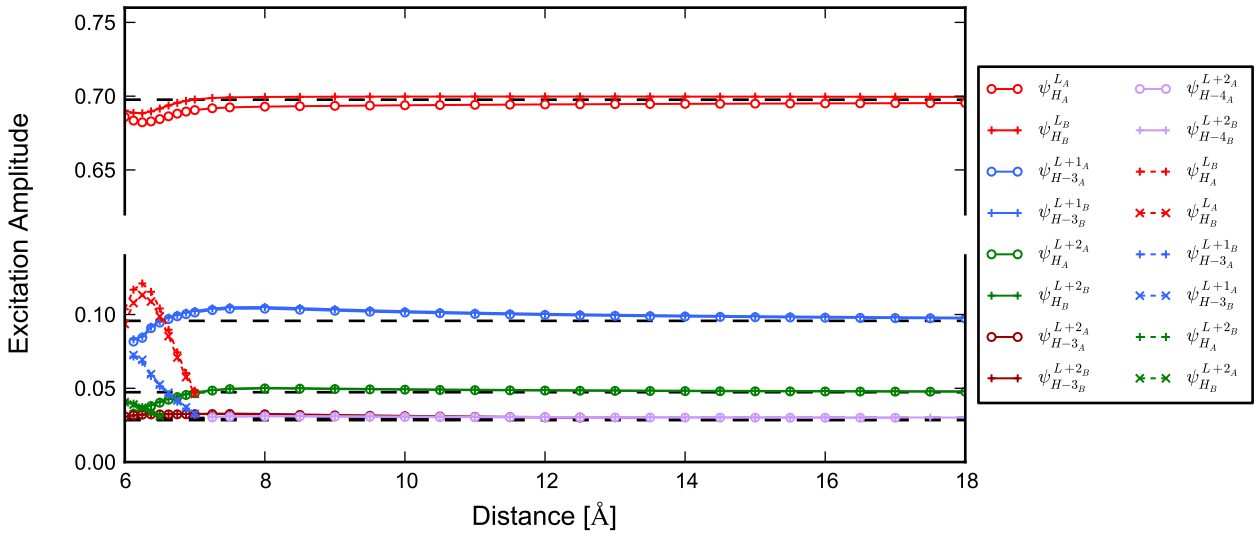

FIG. 7: The expansion coefficients of the parallel-oriented bright state shown as a function of distance. Dashed lines represent the corresponding coefficients in the monomer TDDFT excited states. The top panel shows the dominant single-particle excitation, which corresponds to the excitation of an electron in the highest occupied molecular orbital (HOMO) to the lowest unoccupied molecular orbital (LUMO) of each monomer. The bottom panel shows other single-particle excitations which make up the TDDFT excited state. Molecular orbitals are labeled with respect to their energetic position below the HOMO ($H-n$) or above the LUMO ($L+n$). The excitations that are doubly degenerate (e.g. $\psi^{\mathrm{L}_A}_{\mathrm{H}_A}$ and $\psi^{\mathrm{L}_B}_{\mathrm{H}_B}$) have been averaged and plotted without their molecule index.

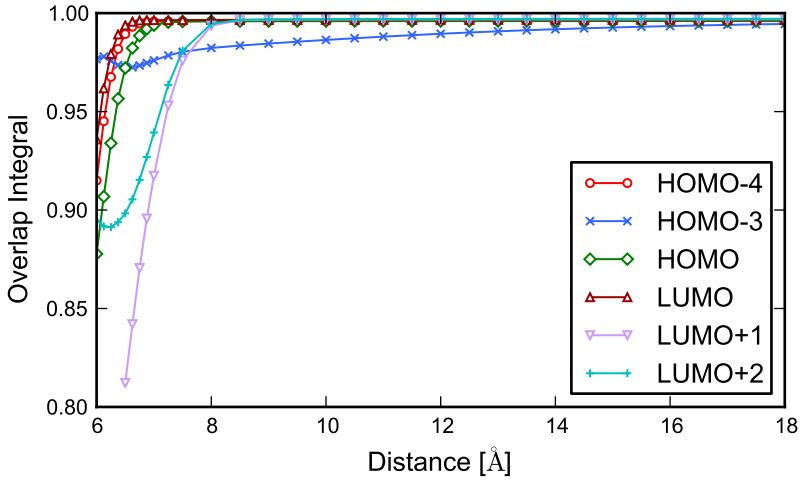

FIG. 8: Overlaps of the bright state dimer molecular orbitals with their corresponding monomer molecular orbitals (See Eq. (11))

perfect for distances greater than 7 Å. Between 6 and 7 Å, these orbitals change by about 8% . Some orbitals change aready at larger distances, such as the LUMO+1 and the LUMO+2 orbitals, which begin to deform as the intermolecular distance is decreased below 8 Å. Finally, the HOMO-3, which with the LUMO+1 forms the next most dominant excitation in the bright state, changes continuously at distances less than 18 Å; however, it changes by only 2% and furthermore it does not form the majority of the excited state, so this effect is diminished in the excited state energies and couplings.

To summarize this investigation of excited state wave functions, we find that for coumarin-343-MA, it is reasonable to describe the dimer wavefunctions in a basis of monomer wavefunctions for separation distances greater than 8 Å. For smaller distances the B3LYP calculations indicate possible mixing in of charge transfer character into the excited state wavefunction, although the extent of this mixing is not conclusive from this level of calculation.

IV. CONCLUSIONS

In this work we have made a critical assessment of the conventional effective Hamiltonian approach of modeling the excitonic properties of molecular aggregates, using the coumarin-343-MA dye as a case study. Results from *ab-initio* electronic structure calculations using TDDFT were compared with predictions from the conventional tight-binding effective Hamiltonian for a homo-dimer (the Heitler-London approximation). Most interestingly, we found that the conventional effective Hamiltonian for a homo-dimer does not reproduce the asymmetric energy splittings calculated using TDDFT. In particular, the ideal dipole approximation of the excited state coupling was found to give a very inaccurate representation of the TDDFT energy splittings. While the TDC method was found to perform much better, both the IDA and the TDC descriptions were found to be unable to reproduce the asymmetric nature of the splitting between bright and dark state energy levels that is predicted from TDDFT. We showed that this is a result of ignoring non-negligible electrostatic energy shifts resulting from the proximity of the two chromophores. We outlined a method for reincorporating these electrostatic shifts using a simple approach that only requires calculating Coulomb integrals based on Mulliken partial atomic charges. This approach is an efficient method for forming more complete effective Hamiltonian descriptions that capture all the relevant physical effects; it only requires TDDFT calculations of dimers of chromophores (of each dimer combination of species present in the aggregate) and the remaining elements are accurately captured by Coulomb integrals. We find that the combination of a TDC description of the transition density coupling together with proper incorporation of electrostatic shifts produces an excellent effective Hamiltonian description of excitonics in molecular aggregates. We also demonstrated the importance of incorporating details of solvent polarity into the molecular aggregate model, since this also determines the degree of influence the electrostatic effects have on excitonic energies.

Additionally, we scrutinized the assumptions of the conventional Heitler-London tight-binding picture of excitonic coupling, by examining changes in the character of the excited state and the coupled molecular orbitals as a function of intermolecular distance. These effects were determined to be small but nonzero for intermolecular distances greater than 7-8 Å, while TDDFT predicts a significant departure from the Heitler-London picture at smaller distances. It also predicts some charge-transfer character at these smaller distances. In the future it would be useful to develop more reliable estimates of this charge-transfer character[7] in order to analyze the interplay between excitonic and charge transfer states in chromophore arrays relevant to natural photosynthesis, such as, e.g., the bacterial reaction center[67].

We expect that our investigation and refinement of effective Hamiltonian descriptions of molecular aggregates will inform the modeling of large molecular aggregates formed by direct aggregation or aggregation by protein templated assembly. Such aggregates show promise as the basis for next-generation light harvesting or sensing devices with tailored properties, and efficient modeling of their excitonic properties through effective Hamiltonians will be important for rational design and engineering of such devices.

Acknowledgments

We thank Matthew Francis and Dan Finley for useful discussions on virus-templated assembly for light harvesting. We thank the Molecular Graphics and Computation Facility at UC-Berkeley for computational resources, which were made possible by the NSF under contract numbers CHE-0233882 and CHE-0840505. Sandia National Laboratories is a multi-program laboratory managed and operated by Sandia Corporation, a wholly owned subsidiary of Lockheed Martin Corporation, for the United States Department of Energy's National Nuclear Security Administration under contract DE-AC04-94AL85000. Financial support for this research was provided by the DARPA QuBE (Quantum Effects in Biological Environments) program under contract number N66001-10-1-4068 and by the NSF (grants CHE-0233882 and CHE-0840505).

Appendix A: Orientation Dependence Calculations

In order to sample the possible dimer orientations, we begin with the molecules held at a fixed intermolecular separation along the x-axis. The transition dipole moment of each molecule is aligned along the z axis, with the plane of the molecule flat on the y-z plane as shown in the Parallel-0° geometry in Fig. 5. The orientation of each molecule can be characterized by the three angles: the roll angle (rotation of the molecule about the transition dipole moment axis), the polar angle θ, and the azimuthal angle ϕ. These three angles correspond to the Euler angles α, β, and γ, respectively. We have found that varying the roll angle does not affect the magnitude of coupling very much, since the roll angle does not change the direction of the transition dipole moment, therefore we do not sample over these angles in the following calculations.

To create our dimer geometries, we first fix the azimuthal angle of molecule A by constraining its transition dipole moment to lie on the x-z plane. We sample over the remaining 3 angular degrees of freedom: the polar angles θ_A and θ_B, and the azimuthal angle ϕ_B. These angles are defined in Fig. 9(a). Next, molecule A is rotated about the y-axis by θ_A, and molecule B is rotated about the $(\hat{y}\cos\phi_B - \hat{x}\sin\phi_B)$ axis by θ_B. In Fig. 9(b), we show examples of the resulting relative orientations possible for two chromophores.

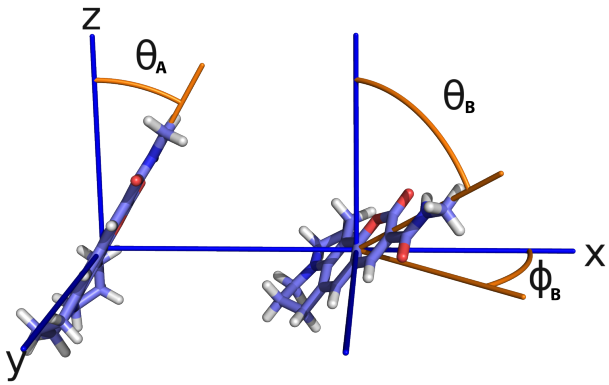

(a) Orientation angles for the chromophores.

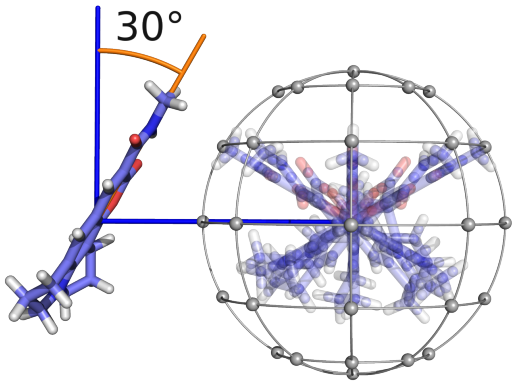

(b) Example of dimer configurations where the polar angle of the first dye is held at 30°, while sweeping over the various relative orientations of the second dye.

FIG. 9: Definition and examples of the three angles used to sample the relative orientations between two molecules.

In Figures 10 – Figure 12, we hold θ_A fixed and plot the coupling as a function of different relative orientations of the second dye. Our sampling scheme leads to 42 possible relative orientations of the second dye. Only half the sphere is shown because the reverse side was found to be quite symmetric due to the high symmetry of charge density across the plane of the page.

The data show that IDA can both over and underestimate the electronic coupling obtained from TDDFT. In general, IDA overestimates for configurations that resemble H-aggregates (when θ_A is 0°) and underestimates for the configurations that resemble J-aggregates (when θ_A is 180°).

Since the IDA is by definition an approximation to the TDC coupling, the over and underestimation of IDA is due to the approximation of using a point dipole to approximate a charge density. The TDC coupling itself seems to perform well over most configurations, giving good agreement with the TDDFT results. There are a few data points for which TDC matches poorly to TDDFT; in these configurations, the spatial extent of the molecules overlaps enough to allow significant interaction between the two molecules.

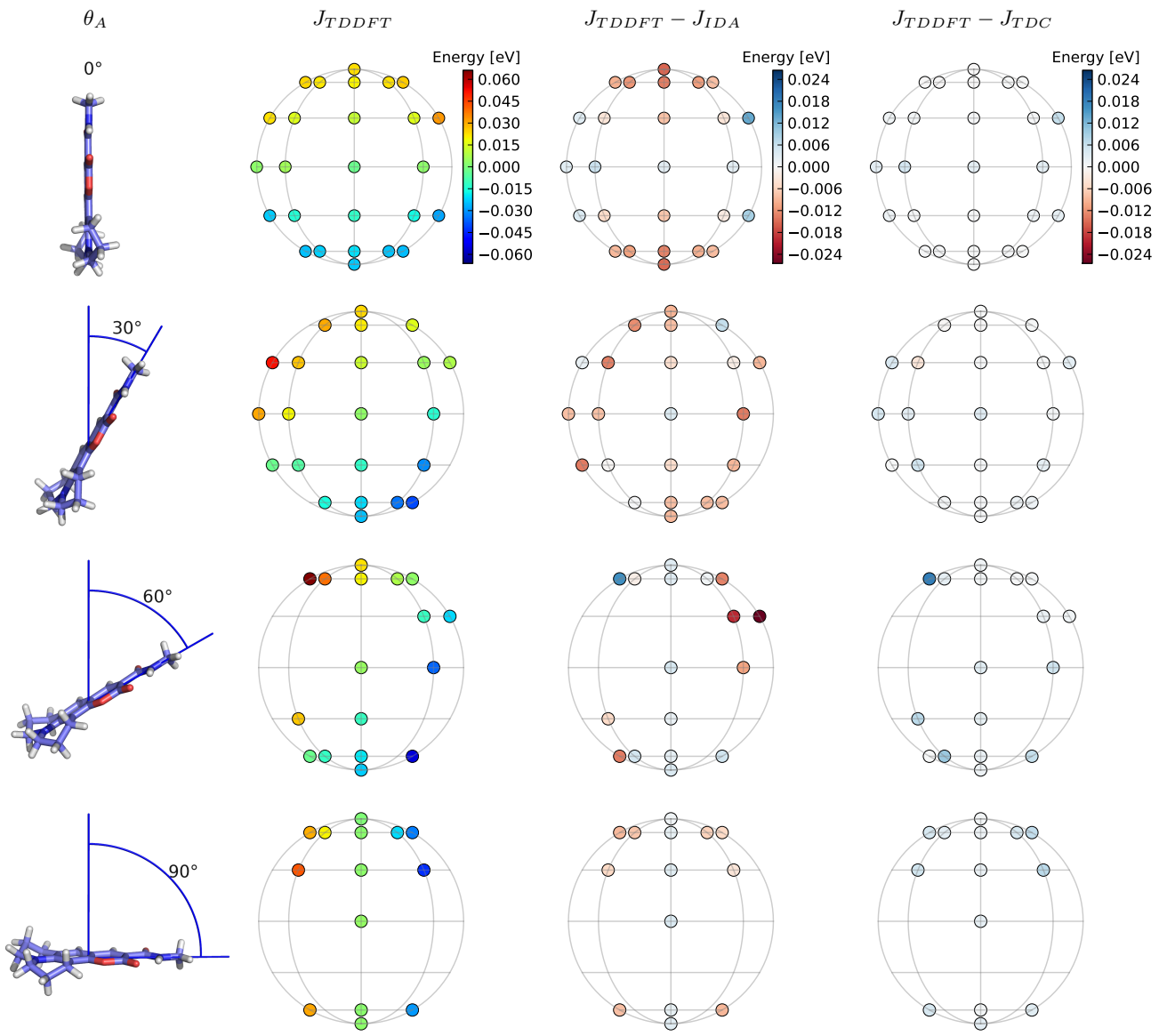

FIG. 10: Dimer relative orientational dependence of electronic coupling at 9 Å separation.
The first column depicts the polar orientation of the first molecule while the position on the polar plots on the right represents the orientation of the second molecule relative to the first (see Fig. 9(b)). Columns 2-4 show the magnitude of J_{TDDFT}, the value of the coupling given by TDDFT (column 2), the error resulting from the IDA approximation to this (column 3) and the error resulting from the TDC estimate (column 4), as a function of the relative orientation.

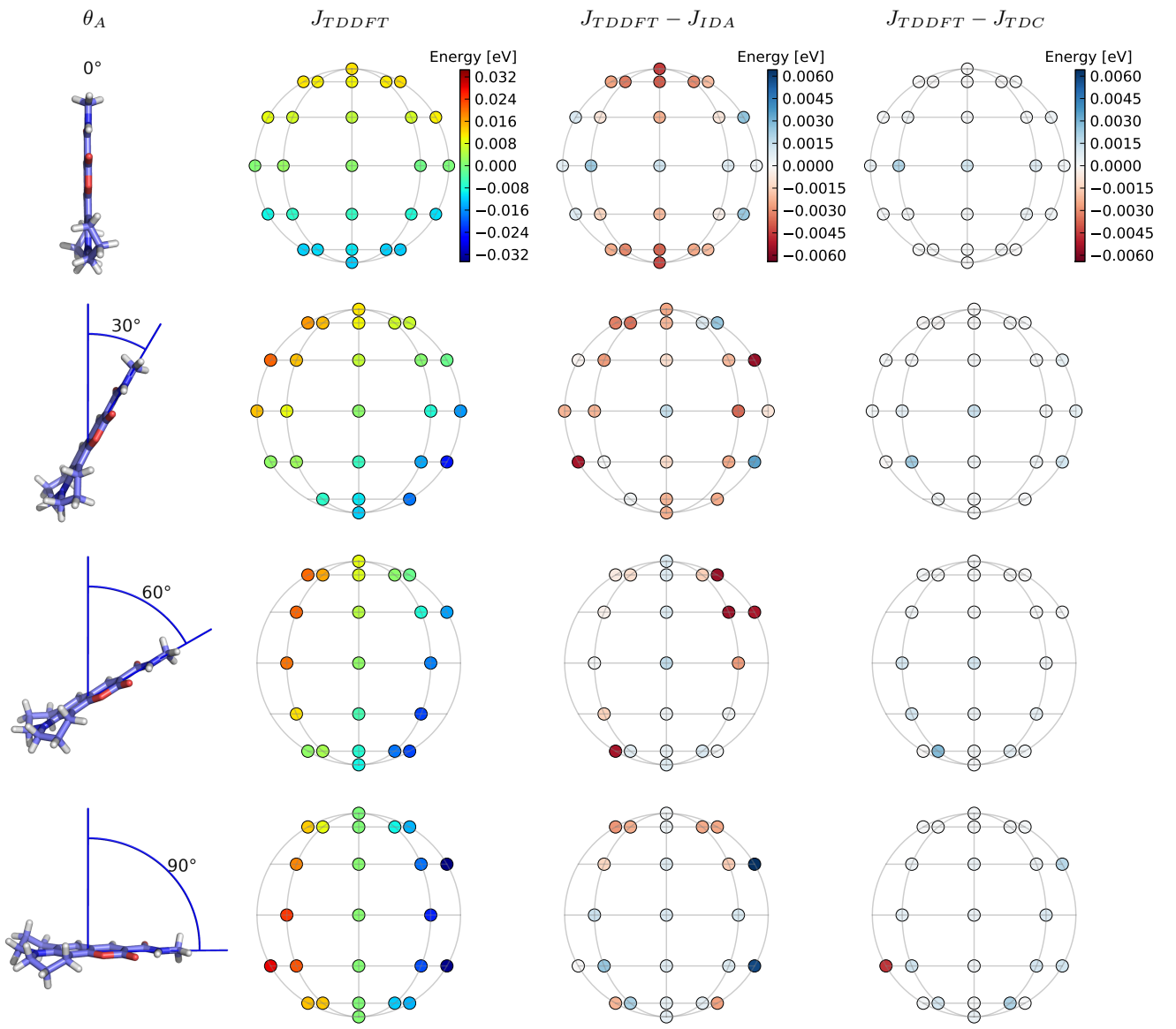

FIG. 11: Dimer relative orientational dependence of electronic coupling at 12 Å separation.
The first column depicts the polar orientation of the first molecule while the position on the polar plots on the right represents the orientation of the second molecule relative to the first (see Fig. 9(b)). Columns 2-4 show the magnitude of J_{TDDFT}, the value of the coupling given by TDDFT (column 2), the error resulting from the IDA approximation to this (column 3) and the error resulting from the TDC estimate (column 4), as a function of the relative orientation.

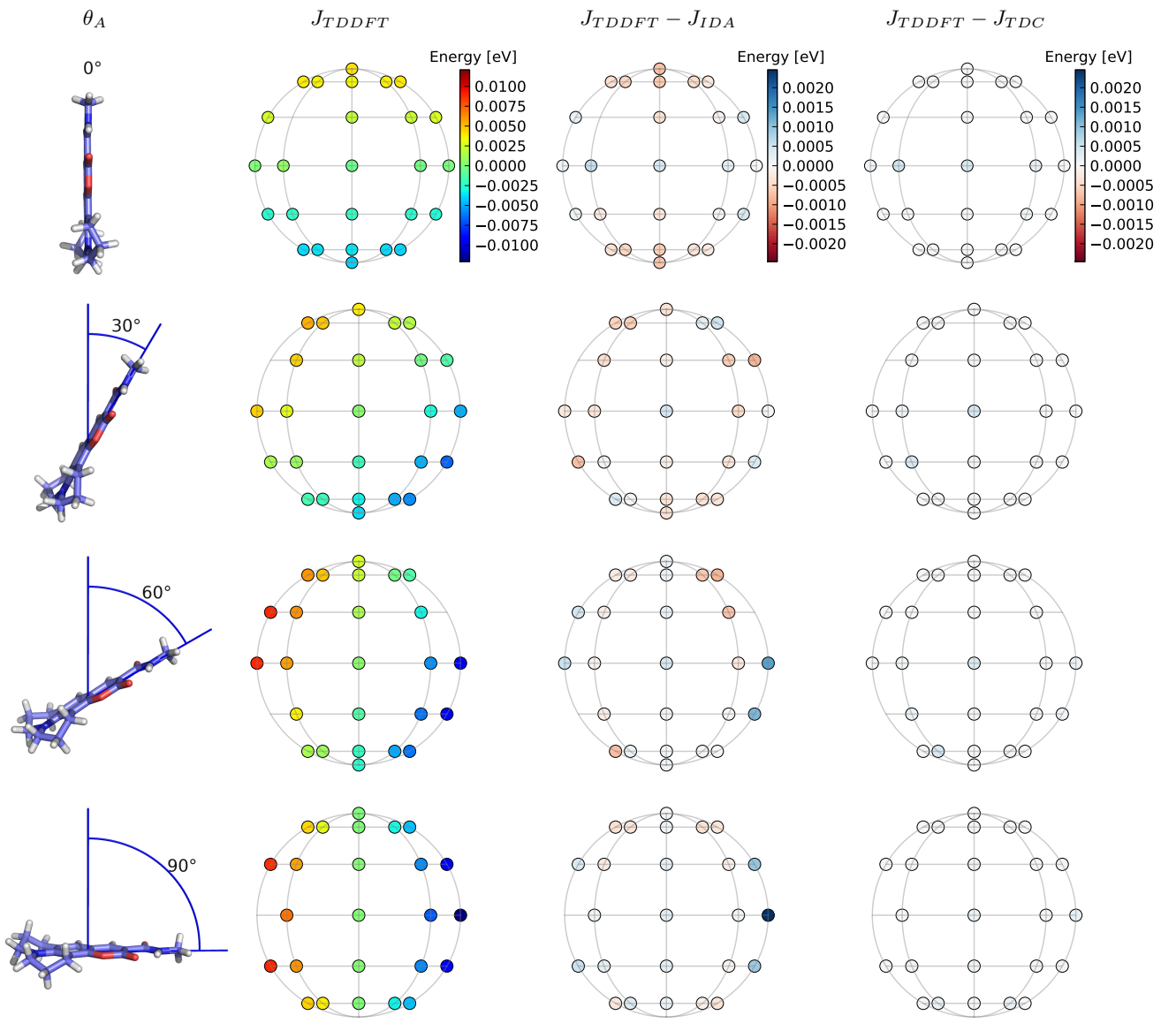

FIG. 12: Dimer relative orientational dependence of electronic coupling at 18 Å separation.
The first column depicts the polar orientation of the first molecule while the position on the polar plots on the right represents the orientation of the second molecule relative to the first (see Fig. 9(b)). Columns 2-4 show the magnitude of J_{TDDFT}, the value of the coupling given by TDDFT (column 2), the error resulting from the IDA approximation to this (column 3) and the error resulting from the TDC estimate (column 4), as a function of the relative orientation.

Appendix B: Charge Transfer states in B3LYP

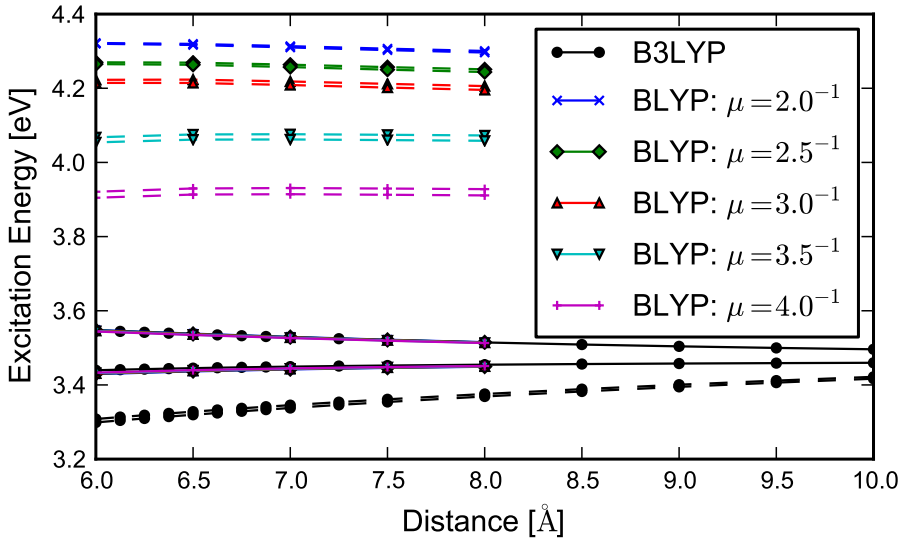

FIG. 13: Coumarin-343 energy levels predicted by B3LYP and range-corrected BLYP. The coupled exciton states (solid lines) for B3LYP and the range corrected calculations are shown overlapped, while the energies of the charge transfer states (dashed lines) varies based on the functional. The range corrected BLYP energies have been shifted such that the first excited state energies of the monomer calculations are all aligned to that of B3LYP. This is done to compare the energies of the charge transfer states relative to the coupled exciton states.

It is well known that TD-B3LYP is poor at predicting the energetics of charge transfer states, as are other functionals without 100% Hartree-Fock exchange[68,69]. Fig. 13 shows that TD-B3LYP predicts low-lying charge transfer states for the coumarin-343-MA dimer. However, the range-corrected DFT calculations show that the charge transfer states are much higher in energy. The splitting between the exciton states is consistent between B3LYP and the range corrected calculations. This suggests that the low lying charge transfer states predicted by B3LYP do not affect the character of the exciton states. Therefore, we may safely disregard these charge transfer states and use only the exciton states in our analysis.

* **Corresponding Author**
E-mail: whaley@berkeley.edu

[1] Scholes, G. D.; Ms, C.; Fleming, G. R. Energy Transfer and Photosynthetic Light Harvesting. In *Advances in Chemical Physics*; Berry, R. S., Jortner, J., Eds.; Advances in Chemical Physics; John Wiley & Sons, Inc.: Hoboken, NJ, USA, 2005; Vol. i; Chapter 2, pp 57–129.
[2] Cheng, Y.-C.; Fleming, G. R. Dynamics of Light Harvesting in Photosynthesis. *Annu. Rev. Phys. Chem.* **2009**, *60*, 241–62.
[3] Scholes, G. D.; Fleming, G. R.; Olaya-Castro, A.; van Grondelle, R. Lessons From Nature About Solar Light Harvesting. *Nat Chem* **2011**, *3*, 763–774.
[4] Blankenship, R. E. *Molecular Mechanisms of Photosynthesis*; Blackwell Science, 2002.
[5] van Amerongen, H.; Valkunas, L.; van Grondelle, R. *Photosynthetic Excitons*; World Scientific, 2000.
[6] Scholes, G. D. Long-Range Resonance Energy Transfer in Molecular Systems. *Annu. Rev. Phys. Chem.* **2003**, *54*, 57–87.
[7] Scholes, G. D. Energy Transfer and Spectroscopic Characterization of Multichromophoric Assemblies. *J. Phys. Chem.* **1996**, *100*, 18731–18739.
[8] Cao, J.; Silbey, R. J. Optimization of Exciton Trapping in Energy Transfer Processes. *J. Phys. Chem. A* **2009**, *113*, 13825–38.
[9] Didraga, C.; Klugkist, J. A.; Knoester, J. Optical Properties of Helical Cylindrical Molecular Aggregates: The Homogeneous Limit. *J. Phys. Chem. B* **2002**, *106*, 11474–11486.
[10] Didraga, C.; Pugžlys, A.; Hania, P. R.; von Berlepsch, H.; Duppen, K.; Knoester, J.; Pugz, A.; Berlepsch, H. V. Structure, Spectroscopy, and Microscopic Model of Tubular Carbocyanine Dye Aggregates. *J. Phys. Chem. B* **2004**, *108*, 14976–14985.

[11] Sarovar, M.; Whaley, K. B. Design Principles and Fundamental Trade-Offs in Biomimetic Light Harvesting. *New J. Phys.* **2013**, *15*, 013030.

[12] Scholes, G. D. Quantum-Coherent Electronic Energy Transfer: Did Nature Think of It First? *J. Phys. Chem. Lett.* **2010**, *1*, 2–8.

[13] Collini, E.; Wong, C. Y.; Wilk, K. E.; Curmi, P. M. G.; Brumer, P.; Scholes, G. D. Coherently Wired Light-Harvesting in Photosynthetic Marine Algae at Ambient Temperature. *Nature* **2010**, *463*, 644–647.

[14] Engel, G. S.; Calhoun, T. R.; Read, E. L.; Ahn, T.-K.; Mancal, T.; Cheng, Y.-C.; Blankenship, R. E.; Fleming, G. R. Evidence for Wavelike Energy Transfer Through Quantum Coherence in Photosynthetic Systems. *Nature* **2007**, *446*, 782–6.

[15] Sarovar, M.; Ishizaki, A.; Fleming, G. R.; Whaley, K. B. Quantum Entanglement in Photosynthetic Light-Harvesting Complexes. *Nat. Phys.* **2010**, *6*, 462–467.

[16] Ma, Y.-Z. Y.-Z.; Miller, R. A.; Fleming, G. R.; Francis, M. B. Energy Transfer Dynamics in Light-Harvesting Assemblies Templated by the Tobacco Mosaic Virus Coat Protein. *J. Phys. Chem. B* **2008**, *112*, 6887–92.

[17] Klug, A. The Tobacco Mosaic Virus Particle: Structure and Assembly. *Phil. Trans. R. Soc. B* **1999**, *354*, 531–5.

[18] Endo, M.; Fujitsuka, M.; Majima, T. Porphyrin Light-Harvesting Arrays Constructed in the Recombinant Tobacco Mosaic Virus Scaffold. *Chemistry (Weinheim an der Bergstrasse, Germany)* **2007**, *13*, 8660–6.

[19] Nam, Y. S.; Shin, T.; Park, H.; Magyar, A. P.; Choi, K.; Fantner, G.; Nelson, K. A.; Belcher, A. M. Virus-Templated Assembly of Porphyrins into Light-Harvesting Nanoantennae. *J. Am. Chem. Soc.* **2010**, *132*, 1462–3.

[20] Miller, R. A.; Presley, A. D.; Francis, M. B. Self-Assembling Light-Harvesting Systems from Synthetically Modified Tobacco Mosaic Virus Coat Proteins. *J. Am. Chem. Soc.* **2007**, *129*, 3104–9.

[21] Witus, L. S.; Francis, M. B. Using Synthetically Modified Proteins to Make New Materials. *Acc. Chem. Res.* **2011**, *44*, 774–83.

[22] Scholes, G. D.; Rumbles, G. Excitons in Nanoscale Systems. *Nat. Mater.* **2006**, *5*, 683–696.

[23] Knoester, J. Optical Properties of Molecular Aggregates. In *Proceedings of the International School of Physics "Enrico Fermi" Course CXLIX*; Agranovich, V. M., LaRocca, G. C., Eds.; Amsterdam: IOS Press, 2002; pp 149–186.

[24] Krueger, B. P.; Scholes, G. D.; Fleming, G. R. Calculation of Couplings and Energy-Transfer Pathways between the Pigments of LH2 by the ab Initio Transition Density Cube Method. *J. Phys. Chem. B* **1998**, *102*, 5378–5386.

[25] Kasha, M.; Rawls, H. R.; Ashraf El-Bayoumi, M. The Exciton Model in Molecular Spectroscopy. *Pure Appl. Chem.* **1965**, *11*, 371–392.

[26] Howard, I. A.; Zutterman, F.; Deroover, G.; Lamoen, D.; Van Alsenoy, C. Approaches to Calculation of Exciton Interaction Energies for a Molecular Dimer. *J. Phys. Chem. B* **2004**, *108*, 19155–19162.

[27] Muñoz Losa, A.; Curutchet, C.; Krueger, B. P.; Hartsell, L. R.; Mennucci, B. Fretting about FRET: Failure of the Ideal Dipole Approximation. *Biophys. J.* **2009**, *96*, 4779–88.

[28] Scholes, G. D.; Jordanides, X. J.; Fleming, G. R. Adapting the Förster Theory of Energy Transfer for Modeling Dynamics in Aggregated Molecular Assemblies. *J. Phys. Chem. B* **2001**, *105*, 1640–1651.

[29] Madjet, M. E.; Abdurahman, a.; Renger, T. Intermolecular Coulomb Couplings from Ab Initio Electrostatic Potentials: Application to Optical Transitions of Strongly Coupled Pigments in Photosynthetic Antennae and Reaction Centers. *J. Phys. Chem. B* **2006**, *110*, 17268–81.

[30] Hsu, C.-P.; Fleming, G. R.; Head-Gordon, M.; Head-Gordon, T. Excitation Energy Transfer in Condensed Media. *J. Chem. Phys.* **2001**, *114*, 3065.

[31] Curutchet, C.; Scholes, G. D.; Mennucci, B.; Cammi, R. How Solvent Controls Electronic Energy Transfer and Light Harvesting: Toward a Quantum-Mechanical Description of Reaction Field and Screening Effects. *J. Phys. Chem. B* **2007**, *111*, 13253–13265.

[32] Sinnokrot, M. O.; Sherrill, C. D. High-Accuracy Quantum Mechanical Studies of Pi-Pi Interactions in Benzene Dimers. *J. Phys. Chem. A* **2006**, *110*, 10656–10668.

[33] Fink, R. F.; Pfister, J.; Schneider, A.; Zhao, H.; Engels, B. Ab Initio Configuration Interaction Description of Excitation Energy Transfer Between Closely Packed Molecules. *Chem. Phys.* **2008**, *343*, 353–361.

[34] Fink, R. F.; Pfister, J.; Zhao, H. M.; Engels, B. Assessment of Quantum Chemical Methods and Basis Sets for Excitation Energy Transfer. *Chem. Phys.* **2008**, *346*, 275–285.

[35] Zhao, H. M.; Pfister, J.; Settels, V.; Renz, M.; Kaupp, M.; Dehm, V. C.; Würthner, F.; Fink, R. F.; Engels, B. Understanding Ground- and Excited-State Properties of Perylene Tetracarboxylic Acid Bisimide Crystals by Means of Quantum Chemical Computations. *J. Am. Chem. Soc.* **2009**, *131*, 15660–15668.

[36] Liu, W.; Settels, V.; Harbach, P. H. P.; Dreuw, A.; Fink, R. F.; Engels, B. Assessment of TD-DFT- and TD-HF-based Approaches for the Prediction of Exciton Coupling Parameters, Potential Energy Curves, and Electronic Characters of Electronically Excited Aggregates. *J. Comput. Chem.* **2011**, *32*, 1971–1981.

[37] Stephens, P. J.; Devlin, F. J.; Chabalowski, C. F.; Frisch, M. J. Ab Initio Calculation of Vibrational Absorption and Circular Dichroism Spectra Using Density Functional Force Fields. *J. Phys. Chem.* **1994**, *98*, 11623.

[38] Ditchfield, R.; Hehre, W. J.; Pople, J. A. Self-Consistent Molecular-Orbital Methods. IX. An Extended Gaussian-Type Basis for Molecular-Orbital Studies of Organic Molecules. *J. Chem. Phys.* **1971**, *54*, 724.

[39] Hehre, W. J.; Ditchfield, R.; Pople, J. A. Self—Consistent Molecular Orbital Methods. XII. Further Extensions of Gaussian—Type Basis Sets for Use in Molecular Orbital Studies of Organic Molecules. *J. Chem. Phys.* **1972**, *56*, 2257.

[40] Hariharan, P.; Pople, J. The Influence of Polarization Functions on Molecular Orbital Hydrogenation Energies. *Theo. Chim. Acta* **1973**, *28*, 213.

[41] Runge, E.; Gross, E. K. U. Density-Functional Theory for Time-Dependent Systems. *Phys. Rev. Lett.* **1984**, *52*, 997.

[42] Gross, E.; Kohn, W. Time-Dependent Density-Functional Theory. In *Density Functional Theory of Many-Fermion Systems*;

Löwdin, P.-O., Ed.; Adv. Quant. Chem.; Academic Press, 1990; Vol. 21; pp 255 – 291.
[43] Zhao, Y.; Truhlar, D. G. Density Functional for Spectroscopy: No Long-Range Self-Interaction Error, Good Performance for Rydberg and Charge-Transfer States, and Better Performance on Average than B3LYP for Ground States. *J. Phys. Chem. A* **2006**, *110*, 13126.
[44] Peverati, R.; Truhlar, D. G. Improving the Accuracy of Hybrid Meta-GGA Density Functionals by Range Separation. *J. Phys. Chem. Lett.* **2011**, *2*, 2810–2817.
[45] Peverati, R.; Truhlar, D. G. M11-L: A Local Density Functional that Provides Improved Accuracy for Electronic Structure Calculations in Chemistry and Physics. *J. Phys. Chem. Lett.* **2012**, *3*, 117–124.
[46] Perdew, J. P.; Burke, K.; Ernzerhof, M. Generalized Gradient Approximation Made Simple. *Phys. Rev. Lett.* **1996**, *77*, 3865–3868.
[47] Perdew, J. P.; Burke, K.; Ernzerhof, M. Generalized Gradient Approximation Made Simple [Phys. Rev. Lett. 77, 3865 (1996)]. *Phys. Rev. Lett.* **1997**, *78*, 1396–1396.
[48] Clark, T.; Chandrasekhar, J.; Spitznagel, G. W.; Schleyer, P. V. R. Efficient Diffuse Function-Augmented Basis Sets For Anion Calculations. III. The 3-21+G Basis Set for First-Row Elements, Li-F. *J. Comput. Chem.* **1983**, *4*, 294.
[49] Krishnan, R.; Binkley, J. S.; Seeger, R.; Pople, J. A. Self-Consistent Molecular Orbital Methods. XX. A Basis Set for Correlated Wave Functions. *J. Chem. Phys.* **1980**, *72*, 650.
[50] Frisch, M. J.; Pople, J. A.; Binkley, J. S. Self-Consistent Molecular Orbital Methods 25. Supplementary Functions for Gaussian Basis Sets. *J. Chem. Phys.* **1984**, *80*, 3265.
[51] Piecuch, P.; Kucharski, S. A.; Kowalski, K.; Musia, M. Efficient Computer Implementation of the Renormalized Coupled-Cluster Methods: The R-CCSD[T], R-CCSD(T), CR-CCSD[T], and CR-CCSD(T) Approaches. *Comput. Phys. Commun.* **2002**, *149*, 71.
[52] Kowalski, K.; Piecuch, P. New Coupled-Cluster Methods With Singles, Doubles, and Noniterative Triples for High Accuracy Calculations of Excited Electronic States. *J. Chem. Phys.* **2004**, *120*, 1715.
[53] Wloch, M.; Gour, J. R.; Kowalski, K.; Piecuch, P. Extension of Renormalized Coupled-Cluster Methods Including Triple Excitations to Excited Electronic States of Open-Shell Molecules. *J. Chem. Phys.* **2005**, *122*, 214107.
[54] Ivanic, J.; Ruedenberg, K. Identification of Deadwood in Configuration Spaces Through General Direct Configuration Interaction. *Theo. Chem. Acc.* **2001**, *106*, 339.
[55] Cossi, M.; Barone, V. Time-Dependent Density Functional Theory for Molecules in Liquid Solutions. *J. Chem. Phys.* **2001**, *115*, 4708.
[56] Tawada, Y.; Tsuneda, T.; Yanagisawa, S.; Yanai, T.; Hirao, K. A Long-Range-Corrected Time-Dependent Density Functional Theory. *J. Chem. Phys.* **2004**, *120*, 8425.
[57] Schmidt, M. W.; Baldridge, K. K.; Boatz, J. A.; Elbert, S. T.; Gordon, M. S.; Jensen, J. H.; Koseki, S.; Matsunaga, N.; Nguyen, K. A.; Su, S.; Windus, T. L.; Dupuis, M.; Montgomery, J. A. General Atomic and Molecular Electronic Structure System. *J. Comput. Chem.* **1993**, *14*, 1347.
[58] M.S.Gordon,; M.W.Schmidt, In *Theory and Applications of Computational Chemistry, the First Forty Years*; C.E.Dykstra,, G.Frenking,, K.S.Kim,, G.E.Scuseria,, Eds.; Elsevier, 2005; p 1167.
[59] Shao, Y. et al. Advances in Methods and Algorithms in a Modern Quantum Chemistry Program Package. *Phys. Chem. Chem. Phys.* **2006**, *8*, 3172.
[60] Löwdin, P.-O. Quantum Theory of Many-Particle Systems. I. Physical Interpretations by Means of Density Matrices, Natural Spin-Orbitals, and Convergence Problems in the Method of Configurational Interaction. *Physical Review* **1955**, *97*, 1474–1489.
[61] Davydov, A. S. The Theory of Molecular Excitons. *Sov. Phys. Usp.* **1964**, *7*, 145–178.
[62] Agranovich, V. *Excitations in Organic Solids*; Oxford University Press, 2008.
[63] Agranovich, V. M.; Basko, D. M. Frenkel excitons beyond the Heitler-London approximation. *J. Chem. Phys.* **2000**, *112*, 8156–8162.
[64] Mulliken, R. S. Electronic Population Analysis on LCAO[Single Bond]MO Molecular Wave Functions. I. *J. Chem. Phys.* **1955**, *23*, 1833.
[65] Madjet, M. E.; Abdurahman, A.; Renger, T. Intermolecular Coulomb Couplings from Ab Initio Electrostatic Potentials: Application to Optical Transitions of Strongly Coupled Pigments in Photosynthetic Antennae and Reaction Centers. *J. Phys. Chem. B* **2006**, *110*, 17268–17281.
[66] Muh, F.; Madjet, M. E.; Adolphs, J.; Abdurahman, A.; Rabenstein, B.; Ishikita, H.; Knapp, E.-W.; Renger, T. α-Helices Direct Excitation Energy Flow in the Fenna-Matthews-Olson Protein. *Proc. Nat. Acad. Sc.* **2007**, *104*, 16862.
[67] Novoderezhkin, V. I.; Yakovlev, A. G.; van Grondelle, R.; Shuvalov, V. A. Coherent Nuclear and Electronic Dynamics in Primary Charge Separation in Photosynthetic Reaction Centers: a Redfield Theory Approach. *J. Phys. Chem. B* **2004**, *108*, 7445–7457.
[68] Dreuw, A.; Head-Gordon, M. Failure of Time-Dependent Density Functional Theory for Long-Range Charge-Transfer Excited States: the Zincbacteriochlorin-Bacteriochlorin and Bacteriochlorophyll-Spheroidene Complexes. *J. Am. Chem. Soc.* **2004**, *126*, 4007–16.
[69] Pan, F.; Gao, F.; Liang, W.; Zhao, Y. Nature of Low-Lying Excited States in H-Aggregated Perylene Bisimide Dyes: Results of TD-LRC-DFT and the Mixed Exciton Model. *J. Phys. Chem. B* **2009**, *113*, 14581–7.